Crystal Structures and Iron Release Properties of Mutants (K206A and K296A) That Abolish the Dilysine Interaction in the N-Lobe of Human Transferrin[†,‡]

Didier Nurizzo,[§] Heather M. Baker,[§] Qing-Yu He,[||] Ross T. A. MacGillivray,[⊥] Anne B. Mason,[||] Robert C. Woodworth,[||] and Edward N. Baker*[,§,@]

School of Biological Sciences and Department of Chemistry, University of Auckland, Auckland, New Zealand, Department of Biochemistry, University of Vermont, Burlington, Vermont 05405, and Department of Biochemistry and Molecular Biology, University of British Columbia, Vancouver, British Columbia V6T 1Z3, Canada

Received August 30, 2000; Revised Manuscript Received December 4, 2000

ABSTRACT: Human transferrin (Tf) is responsible for the binding and transport of iron in the bloodstream of vertebrates. Delivery of this bound iron to cells occurs by a process of receptor-mediated endocytosis during which Tf releases its iron at the reduced endosomal pH of ∼5.6. Iron release from Tf involves a large conformational change in which the two domains that enclose the binding site in each lobe move apart. We have examined the role of two lysines, Lys206 and Lys296, that form a hydrogen-bonded pair close to the N-lobe binding site of human Tf and have been proposed to form a pH-sensitive trigger for iron release. We report high-resolution crystal structures for the K206A and K296A mutants of the N-lobe half-molecule of Tf, hTf/2N, and quantitative iron release data on these mutants and the double mutant K206A/K296A. The refined crystal structures (for K206A, $R = 19.6\%$ and $R_{free} = 23.7\%$; for K296A, $R = 21.2\%$ and $R_{free} = 29.5\%$) reveal a highly conserved hydrogen bonding network in the dilysine pair region that appears to be maintained even when individual hydrogen bonding groups change. The iron release data show that the mutants retain iron to a pH 1 unit lower than the pH limit of wild type hTf/2N, and release iron much more slowly as a result of the loss of the dilysine interaction. Added chloride ions are shown to accelerate iron release close to the pH at which iron is naturally lost and the closed structure becomes destabilized, and to retard it at higher pH.

Serum transferrin (Tf)[1] is a member of a homologous family of proteins, known collectively as the transferrins, that also includes ovotransferrin (oTf), of avian egg white, and lactoferrin (Lf), found in many secretory fluids and in white blood cells. These proteins (*1*, *2*) are characterized by an ability to bind two Fe^{3+} ions, with very high affinity ($K_d \sim 10^{20}$), together with two synergistically bound CO_3^{2-} ions. This gives them the important general role of controlling iron levels in body fluids, thereby protecting against iron-catalyzed free radical formation and limiting bacterial growth. Serum Tf has the additional and critical role of transporting iron in the bloodstream and delivering it to cells by a process of receptor-mediated endocytosis (*3*, *4*). This places an additional requirement on Tf, one in which a mechanism must exist for the release of this tightly bound iron in the acidic endosome.

Structurally, the transferrins have been well characterized (for a review, see ref *2*). They are 80 kDa glycoproteins whose amino acid sequences have a 2-fold internal repeat (∼40% level of sequence identity between their N-terminal and C-terminal halves). Crystal structures of Tf (*5*), Lf (*6*, *7*), and oTf (*8*) show that each protein is folded into two homologous lobes (their N- and C-lobes), with each lobe further divided into two domains with an iron binding site located deep in the interdomain cleft. The iron binding sites are highly conserved; in each protein, the same group of ligands is found in both the N-lobe and C-lobe sites. These comprise two tyrosines, one aspartate, and one histidine (Asp63, Tyr95, Tyr188, and His249 in the N-lobe of human Tf), together with two oxygen atoms from the bidentate carbonate ion.

Both crystallographic (*9*, *10*) and spectroscopic (*11*) studies have shown that iron release from each site is accompanied by a large-scale conformational change in which the domains move apart to open up the binding cleft; in the N-lobes of Lf and Tf, for example, domain rotations of 54° and 60°, respectively, occur (*9*, *10*). What triggers this movement and the release of iron is less clear, however. Crystallographic studies of the N-lobe half-molecule of human transferrin (hTf/2N) at a pH close to that of the acidic endosome have

[†] Supported by grants from the U.S. Public Health Service (RO1-HD20859 to E.N.B. and RO1-DK21739 to R.C.W.), the Marsden Fund of New Zealand, the Health Research Council of New Zealand, and the Wellcome Trust (U.K.) through a Major Equipment Grant.

[‡] Atomic coordinates have been deposited with the Protein Data Bank as entries 1FQE (K206A) and 1FQF (K296A).

* To whom correspondence should be addressed. Phone: (+64) 9-373-7599. Fax: (+64) 9-373-7619. E-mail: ted.baker@auckland.ac.nz.

[§] School of Biological Sciences, University of Auckland.

[||] University of Vermont.

[⊥] University of British Columbia.

[@] Department of Chemistry, University of Auckland.

[1] Abbreviations: Tf, transferrin; Lf, lactoferrin; hTf/2N, recombinant N-terminal half-molecule of human transferrin, residues 1−337; BHK, baby hamster kidney; EDTA, ethylenediaminetetraacetate; Tiron, 4,5-dihydroxy-1,3-benzenedisulfonate; PEG, polyethylene glycol; rms, root-mean-square. Mutants of hTf/2N are designated by the wild type amino acid residue, the sequence number, and the amino acid to which the residue was mutated, e.g., K206A.

10.1021/bi002050m CCC: $20.00
Published on Web 01/19/2001

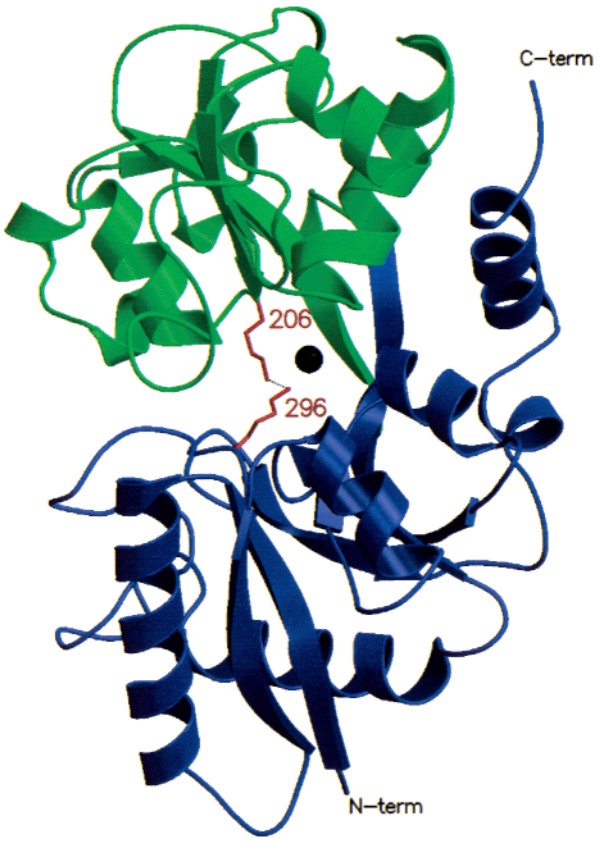

FIGURE 1: Ribbon diagram showing the folding of the wild type hTf/2N molecule and the locations of the side chains of Lys206 and Lys296, hydrogen bonded together, close to the iron binding site. The iron atom is shown as a sphere. In this figure, the N2 domain is at the top of the picture and the N1 domain at the bottom. This structural diagram was drawn with MOLSCRIPT (*41*) and rendered with RASTER3D (*42*).

indicated that protonation of the carbonate ion may be a first step (*12*). Much attention has focused, however, on a pair of lysine residues close to the N-lobe iron binding sites of Tf and oTf. These residues, Lys206 and Lys296 in human Tf and Lys209 and Lys301 in hen oTf, are contributed by opposing domains and form a hydrogen bonding interaction (*12*, *13*) (Figure 1). By implication, only one of the two ϵ-amino groups can be protonated in this interaction, and it has been proposed that protonation of this dilysine pair at lower pH acts as a trigger that stimulates domain opening and iron release, or at least weakens the interactions that hold the domains together (*13*). This could explain why the N-lobes of Tf and oTf release iron at higher pH than their C-lobes, which have no such dilysine pair, and why Lf, which has no equivalent interaction in either lobe, retains iron to a much lower pH (*2*, *13*).

The recombinant N-lobe half-molecule of human Tf, hTf/2N, serves as an excellent model for the N-lobe of the native protein, having very similar spectroscopic, structural, and iron binding and release characteristics (*12*, *14*, *15*). Mutagenesis has thus been used extensively to probe the roles of residues in and around the iron binding site (*15*−*21*). Of particular relevance to iron release, mutation of Lys206 and Lys296 has shown that changes to these residues, and by implication disruption or alteration of the interaction between them, have considerable consequences for the stability of iron binding and rates of iron release. Thus, mutations of Lys206 and Lys296 to Glu or Gln (mutants K206E, K206Q, K296E, and K296Q and the double mutant K206E/K296E) have been shown to increase the stability of iron binding and drastically slow iron release (*20*). Likewise, a study of the mutants K206A and K296A and the double mutant K206A/K296A showed that all retain iron to a lower pH and release iron more slowly than the wild type (*15*, *21*).

Interpretation of the properties of site-specific mutants is made more difficult by the possibility that unexpected structural rearrangements or adjustments may accompany a change in the nature of the mutated amino acid side chains. We have therefore determined high-resolution crystal structures for the K206A and K296A mutants of hTf/2N, and carried out a full, quantitative analysis of their properties of iron binding and release. The crystal structures reveal strong conservation of the environment of the iron binding site and of key hydrogen bonding interactions, and when combined with the iron release data allow a precise definition of the effects of abolition of the dilysine pair interaction on iron binding and release by human transferrin.

MATERIALS AND METHODS

Production of Mutant Proteins. Mutations of Lys206 and Lys296 were introduced into the gene for the N-terminal half-molecule of human transferrin (residues 1−337 of the native protein) using a polymerase chain reaction (PCR)-based procedure (*22*), as described previously (*15*). The mutant proteins were then expressed in baby hamster kidney (BHK) cells, using the pNUT vector, and purified from the tissue culture using procedures that have been described in detail elsewhere (*20*, *23*). Ferric nitrilotriacetate is added to the tissue culture medium during this isolation, and the proteins are thus obtained in their fully iron saturated form. The Fe(III)−hTf/2N samples were then exchanged into 10 mM Hepes (pH 7.4) using Centricon 10 microconcentrators and were stored as concentrated stock solutions (~2.5 mM).

Kinetics of Iron Release. The kinetics of iron removal from the mutant proteins, and the processing of the kinetic data, were carried out as described previously (*18*, *20*). Tiron, at a concentration of 12 mM, was used as the chelator for iron removal at pH 7.4 (in 50 mM Hepes), and EDTA, at a concentration of 4 mM, was used as the chelator at pH 5.6 (in 50 mM Mes). Using these high concentrations of high-affinity, nonsynergistic chelators should preclude any significant back-reaction. The reactions were monitored by following the absorbance increase at 480 nm [for Fe(III)−Tiron] or the absorbance decrease at 293 or 470 nm (for iron removal by EDTA), with a protein concentration of ~40 μM. For the K206A and K296A mutants at pH 5.6, and for the K206A/K296A double mutant at pH 7.4, iron release was very slow, and the rate constants were estimated from a 5 h assay, carried out in duplicate, using the A_{inf} value from the wild type reaction for curve fitting. For the wild type hTf/2N at pH 7.4 and the K206A/K296A double mutant at pH 5.6, the rate of release was moderate, and data were collected for at least four half-lives, resulting in almost complete iron removal. These experiments were carried out using a Cary 219 spectrophotometer under the control of the OLIS-219s program. For the wild type hTf/2N at pH 5.6, release was very rapid and the kinetics were analyzed using an OLIS-RSM 1000 stopped-flow spectrophotometer which

Table 1: Data Collection and Processing

	K206A	K296A
space group	$P2_12_12_1$	$P2_12_12_1$
unit cell (Å)	$a = 43.9$	$a = 44.0$
	$b = 57.3$	$b = 57.0$
	$c = 135.9$	$c = 132.9$
maximum resolution (Å)	1.8	2.1
mosaicity (deg)	0.62	1.20
R_{sym} (%)[a]	7.1 (18.5)	6.2 (30.1)
I/σ[a]	7.4 (3.8)	8.6 (2.4)
no. of unique reflections	29721	19092
multiplicity[a]	3.1 (2.8)	2.9 (2.2)
completeness (%)[a]	91.5 (82.1)	95 (87.1)

[a] Figures in parentheses are for the outermost shell of data (1.90−1.80 Å for K206A and 2.21−2.10 Å for K296A).

is able to record the spectral change in real time. The wavelengths cited above were used as the central wavelength in each assay, with a protein concentration of ∼6.5 μM. All measurements were taken at 25 °C.

Iron Retention Level as a Function of pH. Profiles showing the iron retention level as a function of pH were obtained as described previously (*24*). For each mutant, the fully Fe(III)-loaded protein was incubated against a series of buffers, chosen to give appropriate buffering over the pH range of 7.7−4.2. Each solution was maintained at 4 °C for a period of 1 week to achieve equilibrium. The percentage saturation with iron was then estimated from the visible absorption spectrum, by comparing its absorbance at the visible absorption maximum (458 nm for K206A and 469 nm for K296A) with that of the fully iron saturated protein. All UV−visible spectra were recorded on a Cary 219 spectrophotometer under the control of the OLIS-219s program (On-line Instrument Systems Inc., Bogart, GA).

Crystallization. Crystals of both mutants were grown at room temperature in hanging drops. In each case, the protein solution contained 35 mg/mL mutant (K206A or K296A) in 0.1 M ammonium bicarbonate (pH 7.4), and crystals grew in a period of 4−6 days when 2 μL drops of the protein solution were mixed with 2 μL of reservoir solution that comprised 0.1 M potassium acetate (pH 7.4) containing 20−25% PEG 3350. The red, blocklike crystals of K206A diffracted beyond 1.8 Å resolution. The K296A crystals were poorly formed, however, and suitable crystals were only obtained by microseeding. In this procedure, a freshly crushed crystal was diluted to 100 μL to give a stock suspension of microcrystals; a cat whisker was then dipped into this stock and streaked through a K296A hanging drop pre-equilibrated with a reservoir containing 18% PEG 3350. High-quality crystals, diffracting to 2.0 Å, grew overnight. For both mutants, the crystals were essentially isomorphous with the form 1 wild type hTf/2N crystals: orthorhombic, space group $P2_12_12_1$, with one protein molecule in the asymmetric unit, and cell dimensions as listed in Table 1.

Data Collection and Processing. For both mutants, X-ray diffraction data were collected from flash-frozen crystals at 110 K after the crystals had been transferred to a cryoprotectant comprising 0.1 M potassium acetate (pH 7.4) with 35% PEG 3350. Data for the K206A mutant crystals were collected on beamline 7-1 at the Stanford Synchrotron Radiation Laboratory (Stanford, CA) on a Mar345 imaging plate detector, using a wavelength of 1.08 Å. The first image was indexed, and the programs STRATEGY and TESTGEN (*25*) were used to determine the best data collection strategy. A total of 180 images (0.5° per frame) were collected to give a total oscillation range of 90°. Data for K296A were collected with Cu Kα radiation, with a wavelength of 1.54 Å, using a Rigaku RU-300 rotating anode generator equipped with double-focusing mirrors and a Mar345 imaging plate detector. A total of 100 images (1° per frame) were collected, after using the same protocol as described above to determine the best collection strategy. Both data sets were indexed and integrated using DENZO (*26*) and scaled and merged using programs from the CCP4 suite (*25*). Data sets that were more than 90% complete were obtained, to a maximum resolution of 1.8 and 2.1 Å for the K206A and K296A mutants, respectively. Full statistics are given in Table 1.

Structure Determination. The structures of both mutants were determined using the same protocol, as follows. An initial model was derived from the 1.6 Å resolution wild type hTf/2N structure [form 1, PDB entry 1A8E (*12*)] after removal of all water molecules and the Fe^{3+} and CO_3^{2-} ions; this structure is approximately isomorphous with both mutants. Rigid-body refinement, first as the whole molecule and then as two domains, was carried out with CNS (*27*), followed by simulated annealing between 10 000 and 100 K. SIGMAA-weighted $2mF_o - DF_c$ and $mF_o - DF_c$ difference electron density maps were calculated and were interpreted using the TURBO FRODO graphics package (*28*) on a Silicon Graphics workstation. The positions of the carbonate and ferric ions were clearly apparent and were added to the model. In further cycles of refinement with CNS, water molecules were added automatically and were then visually inspected in SIGMAA-weighted $2mF_o - DF_c$ and $mF_o - DF_c$ maps. Only those sites that had good spherical electron density, reasonable *B*-factors, and hydrogen bond partners with appropriate geometry were retained in the model at each stage. The conformations of the Lys206 (in K296A) and Lys296 (in K206A) side chains were checked at several stages during refinement, with omit maps, and found to have excellent electron density (Figure 2). One solvent molecule in the K206A structure was reassigned as a potassium ion as its environment suggested a cation and its *B*-factor when refined as water was 1 $Å^2$; when the atom was refined as K^+, the *B*-factor assumed a much more reasonable value of 19.5 $Å^2$. The final values for *R* and R_{free} were 19.6 and 23.7% for K206A and 21.2 and 29.5% for K296A, respectively. Approximately 5% of the reflections were used in the R_{free} calculation (*29*), with the same randomly chosen set used for both mutants. Full refinement and model statistics are given in Table 2.

RESULTS AND DISCUSSION

Iron Binding and Release. The iron release kinetic measurements and the pH stability profiles for the K206A and K296A mutants offer complementary data that emphasize the importance of the Lys206−Lys296 interaction in the N-lobe of transferrin. The pH profiles (Figure 3) show that the loss of the dilysine interaction in these mutants causes them to retain iron to a pH significantly lower than the pH limit of wild type hTf/2N. As the pH is lowered, neither mutant begins to lose iron until pH ∼4.5, compared with pH 5.5 for the wild type. Moreover, the two mutants are very similar in this respect; their pH_{50} values (the pH at which 50% of the bound iron remains under these conditions) are

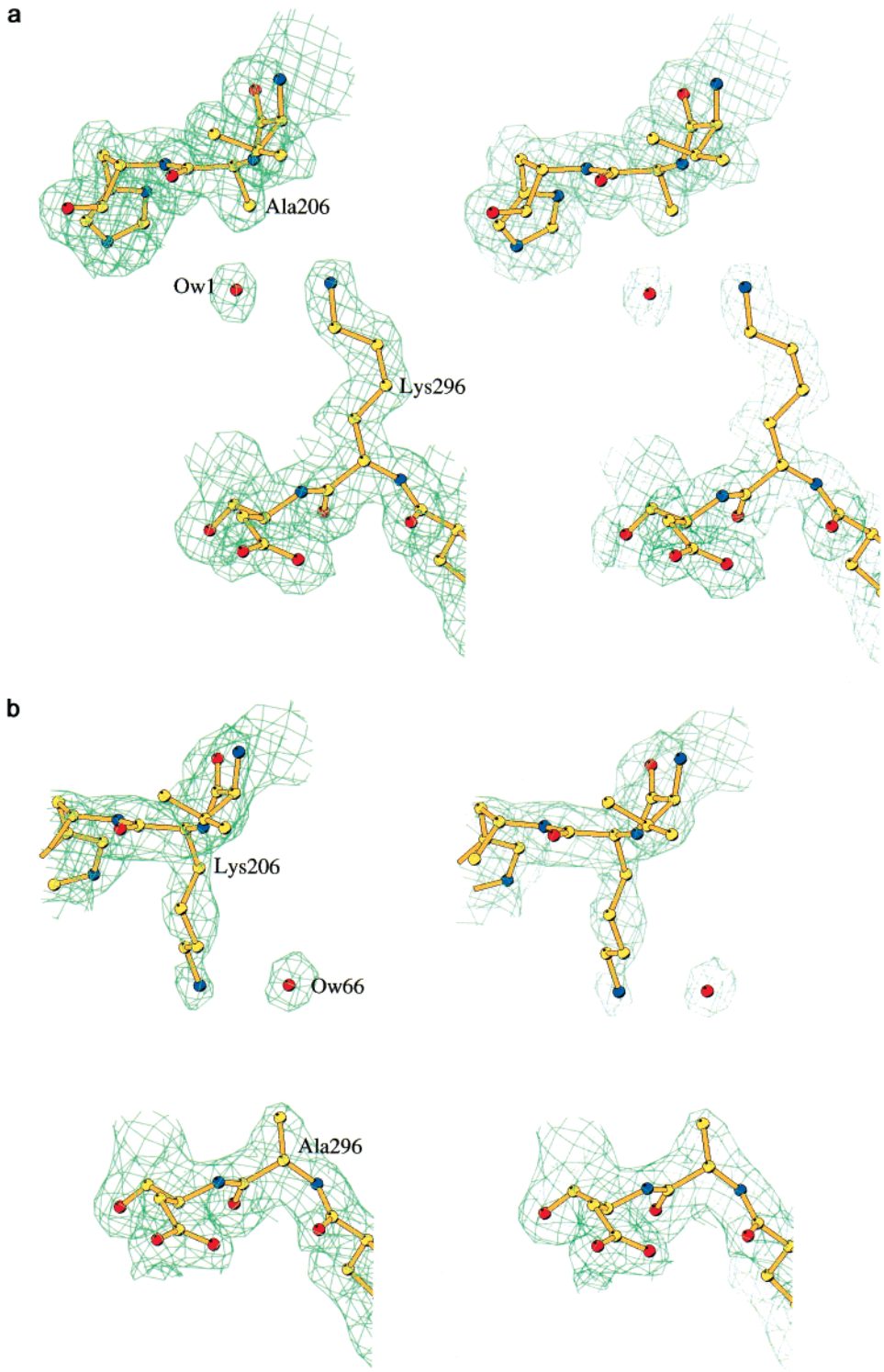

FIGURE 2: Electron density in the region of the mutation sites. (a) The K206A mutant, showing the side chain density for Ala206 and Lys296 and water molecule Ow1 that occupies the site normally filled by Lys206 Nζ. (b) The K296A mutant, showing the side chain density for Lys206 and Ala296 and water molecule Ow66 that fills the site normally occupied by Lys296 Nζ.

3.8 for K206A and 3.9 for K296A, compared with 5.0 for wild type hTf/2N.

The kinetic analyses show that iron release from the K206A and K296A mutants is drastically slowed compared with that from wild type hTf/2N (see Table 3). At pH 7.4, iron release from the mutants is too slow to compare directly with that of the wild type protein, but at pH 5.6, both mutants release iron approximately 10^4 times slower than the wild type. This result is consistent with the observations of Steinlein et al. (*21*) for the same mutants, but provides a more quantitative analysis as the conditions used in the latter study did not allow direct comparison of the mutants and native protein. As for the pH profiles, it is clear that both mutants behave essentially identically under our conditions, implying that the dominant effect is simply the loss of the dilysine interaction, and that it does not matter which one is mutated. The double mutant, K206A/K296A, also releases iron much more slowly than the wild type, but 6-fold faster

Table 2: Model Refinement and Details

	K206A	K296A
resolution limits (Å)	15−1.8	15−2.1
no. of reflections[a]	29721 (1182)	19092 (1055)
R-factor (R_{free}) (%)	19.6 (23.7)	21.2 (29.5)
model details		
no. of protein atoms	2547	2547
no. of ions	Fe^{3+}, CO_3^{2-}, K^+	Fe^{3+}, CO_3^{2-}
no. of solvent molecules	521	502
average temperature factor (Å^2)		
protein main chain atoms	13.7 (0.53)	32.7 (0.80)
protein side chain atoms	15.7 (1.05)	34.5 (1.21)
water molecules	29.9	35.1
rms deviation from ideal geometry		
bond distances (Å)	0.008	0.007
bond angles (deg)	1.4	1.3
residues in most favored regions of the Ramachandran plot (%)	87.1	86.4

[a] All data used, with no σ cutoff.

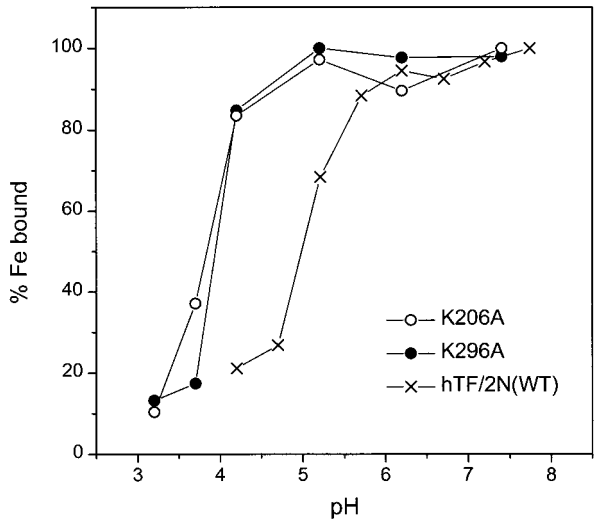

FIGURE 3: pH profiles for iron release from wild type hTf/2N and the K206A and K296A mutants. In each case, the percent of iron saturation is shown as a function of pH (for experimental details, see the text). Wild type data from ref *24*.

than the individual mutants; this emphasizes the fact that the main effect still results from the loss of the dilysine interaction, but the loss of some other, stabilizing, interactions diminishes the effect slightly.

The effect of added chloride is especially interesting. At pH 5.6, iron release is slightly retarded for both single mutants, and the double mutant, in the presence of increased chloride, an effect that has also been observed when Lys206 or Lys296 is changed to Glu or Gln (*20*). In contrast, for the wild type protein, the same concentration of Cl^- enhances iron release. Comparison with the wild type protein at the higher pH of 7.4 suggests a probable explanation. At pH 7.4, added chloride has been shown to retard iron release from the wild type, just as occurs for the mutants at pH 5.6. This suggests that when the protein is far from its intrinsic pH of iron release, at which release occurs in the absence of chelators, chloride has a slight stabilizing effect, i.e., for wild type hTf/2N at pH 7.4 and the K206A and K296A mutants at pH 5.6. On the other hand, when the protein is close to its intrinsic pH of iron release (e.g., wild type at pH 5.6), chloride accelerates iron release. This is consistent with the hypothesis that the accelerating effect of chloride is expressed only under conditions that favor cleft opening (*30*).

There are two ways in which anions such as chloride could accelerate loss of iron close to the "intrinsic" pH of iron release. First, even in the closed form of the protein, small ions should be able to access the binding cleft, which is solvent-filled (*7*, *8*, *12*). Binding to key groups could then enhance cleft opening if it is already susceptible. Second, even after cleft opening, the iron may remain associated with just one domain in a manner similar to the intermediate characterized by Mizutani et al. (*31*). Anion binding at nearby sites could then accelerate the final breakup of such an intermediate.

As the pH is lowered, at least three protonation events occur, involving the metal-bound carbonate ion, the dilysine pair, and the liganding His249, and any or all of these could provide chloride binding sites. It appears that multiple binding sites are involved in the binding of anions (including Cl^-) since no mutation to date has led to the complete abrogation of the salt effect. Multiple sulfate binding sites have also been demonstrated crystallographically for the open, apo form of the N-lobe of oTf, including two sites that may have direct relevance to iron release, the synergistic anion site and the iron ligand His250 (*32*).

In the N-lobe of Tf, protonation of the carbonate ion causes it to become detached from its binding site (*12*) and added chloride ions could accelerate this process by competing for the synergistic anion binding site, thus enhancing iron release. This site should be accessible in either the open or closed form since the side chain of Arg124 is largely solvent-exposed within the cleft. Protonation of Lys206 and/or Lys296 or the histidine ligand could provide additional binding sites for chloride. The importance of the Lys206/Lys296 pair as an anion-binding site in the apo form of hTf/2N has been shown by mutagenesis (*20*), and the histidine ligand, His249, is suggested as an anion binding site by analogy with oTf (*32*).

It is not clear what is responsible for the slight retarding effect of chloride on iron release at higher pH. At higher pH, the favored sites for anion binding may well be different, but whether there are specific stabilizing sites or whether the effect is a more general one is not known. At higher pH, away from the pH at which protonation begins to destabilize the closed form of the protein, iron release only occurs through the intervention of suitable chelating molecules. Competition with salt may then lead to a reduction in the effective chelator concentration at the protein surface.

Structures of K206A and K296A. In both mutant structures, the polypeptide is complete, from Asp3 through to Cys331, i.e., only residues 1, 2, and 332−337 are missing from the model. In each mutant, the rest of the protein exhibits well-defined electron density, and conforms well with standard geometry; for K206A, 87.1% of residues have main chain torsion angles in the most favorable regions of the Ramachandran plot, as defined in the program PROCHECK (*33*), and for K296A, the figure is similar, 86.4%.

The polypeptide folding is essentially unaltered in the two mutants, and there are no significant differences in their detailed structures, compared with the wild type protein (*12*). When K296A is superimposed on wild type hTf/2N (using the orthorhombic form 1 structure, PDB entry 1A8E), the whole molecule matches with a root-mean-square (rms) difference in Cα positions of 0.42 Å (for 320 Cα atoms,

Table 3: Iron Binding and Release Data[a]

	hTf/2N	K206A	K296A	K206A/K296A
λ_{max} (nm)	472	458	469	470
rate constants k (min^{-1})[b]				
pH 5.6, [Cl^-] = 0	4.99 (8)	0.00403	0.00410	0.0248 (15)
pH 5.6, [Cl^-] = 50 mM	22.6 (8)	0.00317	0.00295	0.0188 (5)
pH 7.4, [Cl^-] = 0	0.0225 (9)	too slow	too slow	0.000436
pH 7.4, [Cl^-] = 50 mM	0.0205 (4)	too slow	too slow	0.000136

[a] Values for the wild type protein and for K206A/K296A taken from ref *30*. [b] Standard deviations (in parentheses) obtained from the spread of four replicate measurements.

Table 4: Metal−Ligand Bond Lengths (Å)

	hTf/2N[a]	K206A	K296A
M−Oδ1 (Asp63)	2.02	2.12	2.05
M−Oη (Tyr95)	1.99	1.98	2.09
M−Oη (Tyr188)	1.90	2.07	2.00
M−Nϵ2 (His249)	2.10	2.15	2.06
M−O1 (CO_3^{2-})	2.06	2.22	2.34
M−O2 (CO_3^{2-})	2.24	2.17	1.73

[a] Data from the high-pH structure for form 1 hTf/2N crystals (*12*).

omitting the five N-terminal residues and 10 C-terminal residues). Using the individual domains, the rms differences are 0.37 Å for the N1 domain and 0.33 Å for the N2 domain. Likewise, for K206A, comparison with wild type hTf/2N gives an rms difference of 0.37 Å for the whole molecule, 0.31 Å for the N1 domain, and 0.28 Å for the N2 domain. From comparison of the whole-molecule and individual-domain figures, it is clear that neither mutation is associated with any significant difference in domain orientations. One novel feature in the K206A structure is the presence of a bound potassium ion, which presumably derives from the potassium acetate buffer used in crystallization. This K^+ ion is bound to a surface loop of the N2 domain, coordinated to the carbonyl oxygen atoms of residues 151, 152, and 154, the Oϵ1 atom of Gln169, and two waters which complete a distorted octahedral site.

Iron Binding Sites. No significant change is apparent in the iron binding site of either mutant, when compared with wild type hTf/2N (Table 4). The small differences in the energy of the Fe−O(Tyr) interaction, inferred from the differences in the wavelength of the visible absorption maximum (472, 458, and 469 nm for the wild type, K206A, and K296A, respectively), are not reflected in any obvious differences in the Fe−O(Tyr) bond lengths. For both mutants, the carbonate ion is bound as a bidentate ligand to the metal, and completes the same set of hydrogen bonds that is characteristic of lactoferrin (*34*) and ovotransferrin (*8*). Since the K206A and K296A crystals were grown at pH 7.4, this carbonate binding mode, which corresponds with the high-pH binding mode inferred from wild type hTf/2N crystals (*12*), clearly represents the physiological binding mode for transferrin. Geometrically favorable hydrogen bonds are formed with Thr120, Arg124, and the N-terminus of helix 5. The carbonate ion does appear to be asymmetrically bound in K296A, but we cannot offer an explanation for this at the present time.

Structural Conservation in the Mutation Sites. The region surrounding Lys206 and Lys296 remains remarkably unaltered by the mutation of either Lys206 or Lys296 (see Figure 4). In K206A, the conformation of the remaining lysine, Lys296, remains exactly as in wild type hTf/2N, with the same side chain torsion angles (rms difference of 4.7°) and the ϵ-amino group hydrogen bonded to Tyr188 Oη and two water molecules; one of the latter is hydrogen bonded to Ser208 Oγ and Ser298 Oγ (as in the wild type), whereas the other (Ow1) occupies the position that is filled by Lys206 Nζ in the wild type protein. Likewise, in K296A, the conformation of Lys206 remains as in the wild type (rms difference in torsion angles of 13.2°), with its ϵ-amino group hydrogen bonded to Ser298 Oγ and two water molecules; one of the latter (Ow66) occupies the site filled by Lys296 Nζ in hTf/2N. The correspondence of positions in this region of this wild type and mutant proteins (Figure 4) is remarkable, with Ow1 in K206A only 0.72 Å from the site that would be filled by Lys296 Nζ and Ow66 in K296A only 0.33 Å from that normally occupied by Lys206 Nζ. This conservation of structure also extends to the K206Q mutant of hTf/2N (*35*), in which the side chain of Gln206 closely aligns with that of Lys206 in the wild type, and the Oϵ1 atom of Gln206 occupies the site of Lys206 Nζ.

The conservation of side chain structures and of atomic positions between wild type hTf/2N and the three lysine mutants (K206Q, K206A, and K296A) has two important implications. First, it is associated with a highly conserved network of hydrogen bonds, described below, and second, it implies that mutational studies in which these residues are changed can be interpreted with the expectation that changes to the protein structure are minimal and predictable.

Conserved Hydrogen Bonding Network in the Dilysine Pair Region of Tf. The conservation of the orientations of Lys206 and Lys296 is associated with a highly conserved hydrogen bonding network that appears to be present in all transferrins. For example, the dilysine pair interaction between Lys206 Nζ and Lys296 Nζ in hTf/2N is replaced with a Lys296 Nζ···water hydrogen bond in K206A, a Lys296 Nζ···Gln206 Oϵ1 hydrogen bond in K206Q, and a Lys206 Nϵ···water hydrogen bond in K296A. Likewise, the Tyr188 Oη···Lys296 Nζ hydrogen bond found in hTf/2N, K206A, and K206Q is replaced with a Tyr188 Oη..···water interaction in K296A. In the H249E mutant of hTf/2N, when the side chain of Lys296 moves to ion pair with the introduced Glu249, its Nζ atom replaces a water molecule present in the wild type protein, and the position vacated by Lys296 Nζ is again filled by a water (*24*). Similar conservation has been noted in the equivalent hydrogen bonding network in Lf, in response to mutations (*36*) or sequence variations between different species (*37*). We conclude that this hydrogen bonding network is highly conserved and important, and that any change in hydrogen bonding atoms is made up by the introduction of others, if necessary from bound water, to preserve the essential structure of this region, close to the iron site.

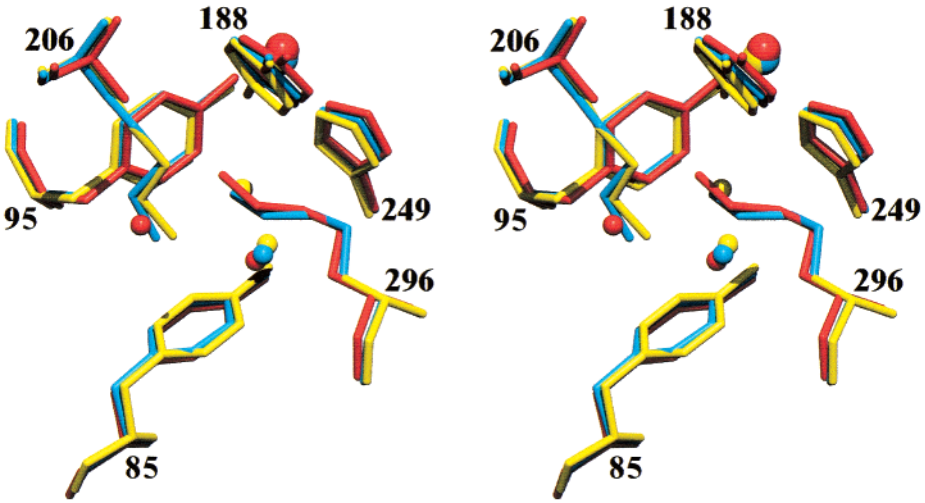

FIGURE 4: Stereoview showing the conservation of structure in the vicinity of the dilysine residues, Lys206 and Lys296, in the human transferrin N-lobe. Wild type hTf/2N is shown in blue, K206A in red, and K296A in yellow. The side chain aromatic rings of Tyr85, Tyr95, Tyr188, and His249 surrounding the two lysines are undisturbed in the mutants as are the iron atoms (large sphere at the top of the picture). In K296A, a water molecule (yellow sphere) fills the site usually occupied by the Lys296 amino group, and in K206A, a water molecule (red sphere) fills the site usually occupied by the Lys206 amino group. These structural diagrams were drawn with MOLSCRIPT (*41*) and rendered with RASTER3D (*42*)

Cation−π Interactions. A feature of the dilysine pair region in all transferrins is that the two basic side chains are surrounded by a cluster of aromatic residues (Figure 4) with which they make an intimate network of interactions (*12*, *13*, *21*, *38*). In the N-lobe of human transferrin, these are the two tyrosine ligands, Tyr95 and Tyr188, the histidine ligand, His249, and second-shell residues Tyr85 and His207. Using a cutoff distance of 6 Å and computing the distance to the centroid of each ring, the ϵ-amino group of Lys206 is within 6 Å of the aromatic rings of Tyr85 (4.1 Å), Tyr95 (4.5 Å), His207 (5.3 Å), and Tyr188 (6.0 Å) in the hTf/2N structure. Likewise, the ϵ-amino group of Lys296 is surrounded by the rings of Tyr95 (3.4 Å), Tyr85 (4.1 Å), His249 (4.2 Å), and Tyr188 (4.8 Å). These interactions in hTf/2N are best described as cation−π interactions (*39*) rather than as amino−aromatic hydrogen bonds (*40*) because the angles are inappropriate for hydrogen bonds.

Cation−π interactions can make a significant contribution to stability (*39*) and are known to stabilize the protonation of basic residues. This has several implications for the mutants in our study. The K206A and K296A structures show that in each case the cation−π interactions of the nonmutated lysine are maintained (Figure 4). Thus, we provide experimental evidence that the mutation of either Lys206 or Lys296 to Ala results in the loss of a set of cation−π interactions, and infer that in the case of the double mutant K206A/K296A, both sets of interactions must be lost. This could explain why, as first suggested by Steinlein et al. (*21*), the double mutant releases iron more rapidly than either single mutant, and why both single mutants are roughly equivalent. A second implication is that the absence of the dilysine pair interaction in the mutants, which results in greater stability at low pH, is in some degree counterbalanced by the destabilizing loss of some cation−π interactions.

CONCLUSIONS

The crystal structures of the K206A and K296A mutants of hTf/2N show that these mutations do not cause any conformational changes in the protein, either in the arrangement of its two domains or in the detailed structure of the iron binding site and its surroundings. In fact, there is strong conservation of the hydrogen bonding network associated with the metal site, with water molecules replacing the missing lysine ϵ-amino groups in the two mutants. This means that the altered functional properties of the two mutants can be attributed directly to the chemical changes introduced via the mutations and not to unexpected structural change. The equilibrium iron release experiments show that the loss of the dilysine interaction, from mutation of either lysine, allows the protein to retain iron to a significantly lower pH, by about 1 pH unit. This emphasizes the contribution of the dilysine pair in facilitating iron release at the physiologically relevant pH of 5.6. Significantly, the kinetic studies of iron release show that not only is iron release drastically slowed in the absence of the dilysine interaction but also the ability of added chloride to enhance release at pH 5.6 is lost. We conclude that for the lysine mutants pH 5.6 is too far from their pH of intrinsic iron release (pH ∼4.5) for anions to have an accelerating effect. This supports the hypothesis that anions enhance iron release from the N-lobe of Tf only under conditions of pH that already favor cleft opening (*30*).

ACKNOWLEDGMENT

We gratefully acknowledge Ty Adams for first identifying the high-pH crystallization conditions used here, Richard Kidd, Clyde Smith, and Andrew McCarthy for help with data collection, and staff at the Stanford Synchrotron Radiation Laboratory for facilitating the collection of synchrotron data.

REFERENCES

1. Aisen, P., and Harris, D. C. (1989) in *Iron carriers and iron proteins* (Loehr, T., Ed.) pp 241−351, VCH Publishers, New York.
2. Baker, E. N. (1994) *Adv. Inorg. Chem. 41*, 389−463.
3. Klausner, R. D., Ashwell, J. V., Van Renswoude, J. B., Harford, J., and Bridges, K. (1983) *Proc. Natl. Acad. Sci. U.S.A. 80*, 2263−2267.

4. Aisen, P. (1998) *Metal Ions Biol. Syst. 35*, 585−631.
5. Bailey, S., Evans, R. W., Garratt, R. C., Gorinsky, B., Hasnain, S., Horsburgh, C., Jhoti, H., Lindley, P. F., Mydin, A., Sarra, R., and Watson, J. L. (1988) *Biochemistry 27*, 5804−5812.
6. Anderson, B. F., Baker, H. M., Dodson, E. J., Norris, G. E., Rumball, S. V., Waters, J. M., and Baker, E. N. (1987) *Proc. Natl. Acad. Sci. U.S.A. 84*, 1769−1773.
7. Anderson, B. F., Baker, H. M., Norris, G. E., Rice, D. W., and Baker, E. N. (1989) *J. Mol. Biol 209*, 711−734.
8. Kurokawa, H., Mikami, B., and Hirose, M. (1995) *J. Mol. Biol. 254*, 196−207.
9. Anderson, B. F., Baker, H. M., Norris, G. E., Rumball, S. V., and Baker, E. N. (1990) *Nature 344*, 784−787.
10. Jeffrey, P. D., Bewley, M. C., MacGillivray, R. T. A., Mason, A. B., Woodworth, R. C., and Baker, E. N. (1998) *Biochemistry 37*, 13978−13986.
11. Grossmann, J. G., Neu, M., Pantos, E., Schwab, F. J., Evans, R. W., Towns-Andrews, E., Lindley, P. F., Appel, H., Thies, W.-G., and Hasnain, S. S. (1992) *J. Mol. Biol. 225*, 811−819.
12. MacGillivray, R. T. A., Moore, S. A., Chen, J., Anderson, B. F., Baker, H., Luo, Y., Bewley, M., Smith, C. A., Murphy, M. E., Wang, Y., Mason, A. B., Woodworth, R. C., Brayer, G., and Baker, E. (1998) *Biochemistry 37*, 7919−7928.
13. Dewan, J. C., Mikami, B., Hirose, M., and Sacchettini, J. C. (1993) *Biochemistry 32*, 11963−11968.
14. Funk, W. D., MacGillivray, R. T. A., Mason, A. B., Brown, S. A., and Woodworth, R. C. (1990) *Biochemistry 29*, 1654−1660.
15. Li, Y., Harris, W. R., Maxwell, A., MacGillivray, R. T. A., and Brown, T. (1998) *Biochemistry 37*, 14157−14166.
16. Woodworth, R. C., Mason, A. B., Funk, W. D., and MacGillivray, R. T. A. (1991) *Biochemistry 30*, 10824−10829.
17. Zak, O., Aisen, P., Crawley, J. B., Joannou, C. L., Patel, K. J., Rafiq, M., and Evans, R. W. (1995) *Biochemistry 34*, 14428−14434.
18. He, Q.-Y., Mason, A. B., Woodworth, R. C., Tam, B. M., Wadsworth, T., and MacGillivray, R. T. A. (1997) *Biochemistry 36*, 5522−5528.
19. He, Q.-Y., Mason, A. B., Woodworth, R. C., Tam, B. M., MacGillivray, R. T. A., Grady, J. K., and Chasteen, N. D. (1998) *J. Biol. Chem. 273*, 17018−17024.
20. He, Q.-Y., Mason, A. B., Tam, B. M., MacGillivray, R. T. A., and Woodworth, R. C. (1999) *Biochemistry 38*, 9704−9711.
21. Steinlein, L. M., Ligman, C. M., Kessler, S., and Ikeda, R. A. (1998) *Biochemistry 37*, 13696−13703.
22. Nelson, R. M., and Long, G. L. (1989) *Anal. Biochem. 180*, 147−151.
23. Mason, A. B., Funk, W. D., MacGillivray, R. T. A., and Woodworth, R. C. (1991) *Protein Expression Purif. 2*, 214−220.
24. MacGillivray, R. T. A., Bewley, M. C., Smith, C. A., He, Q.-Y., Mason, A. B., Woodworth, R. C., and Baker, E. N. (2000) *Biochemistry 39*, 1211−1216.
25. Collaborative Computational Project No. 4 (1994) *Acta Crystallogr., Sect. D 50*, 760−763.
26. Otwinowski, Z., and Minor, W. (1997) *Methods Enzymol. 276*, 307−326.
27. Brunger, A. T., Adams, P. D., Clore, G. M., Delano, W. L., Gros, P., Grosse-Kunstleve, R. W., Jiang, J. S., Kussweski, J., Nilges, M., Pannu, N. S., Read, R. J., Rice, L. M., Simonson, T., and Warren, G. L. (1998) *Acta Crystallogr., Sect. D 54*, 905−921.
28. Cambillau, C., Roussel, A., Inisan, A.-G., and Knoops-Mouthuy, E. (1996) *Bio-Graphics*, AFMB-CNRS, Marseille, France.
29. Brunger, A. T. (1992) *Nature 355*, 472−474.
30. He, Q.-Y., Mason, A. B., Nguyen, V., MacGillivray, R. T. A., and Woodworth, R. C. (2000) *Biochem. J. 350*, 909−915.
31. Mizutani, K., Yamashita, H., Kurokawa, H., Mikami, B., and Hirose, M. (1999) *J. Biol. Chem. 274*, 10190−10194.
32. Mizutani, K., Yamashita, H., Mikami, B., and Hirose, M. (2000) *Biochemistry 39*, 3258−3265.
33. Laskowski, R. A., MacArthur, M. W., Moss, D. S., and Thornton, J. M. (1993) *J. Appl. Crystallogr. 26*, 283−291.
34. Haridas, M., Anderson, B. F., and Baker, E. N. (1995) *Acta Crystallogr., Sect. D 51*, 629−646.
35. Yang, A. H.-W., MacGillivray, R. T. A., Chen, J., Luo, Y., Wang, Y., Brayer, G. D., Mason, A. B., Woodworth, R. C., and Murphy, M. E. P. (2000) *Protein Sci. 9*, 49−52.
36. Peterson, N. A., Anderson, B. F., Jameson, G. B., Tweedie, J. W., and Baker, E. N. (2000) *Biochemistry 39*, 6625−6633.
37. Moore, S. A., Anderson, B. F., Groom, G. R., Haridas, M., and Baker, E. N. (1997) *J. Mol. Biol. 274*, 222−236.
38. Day, C. L., Anderson, B. F., Tweedie, J. W., and Baker, E. N. (1993) *J. Mol. Biol. 232*, 1084−1100.
39. Dougherty, D. A. (1996) *Science 271*, 163−168.
40. Burley, S. K., and Petsko, G. A. (1986) *FEBS Lett. 203*, 139−143.
41. Kraulis, P. J. (1991) *J. Appl. Crystallogr. 24*, 946−950.
42. Merritt, E. A., and Murphy, M. E. P. (1994) *Acta Crystallogr., Sect. D 50*, 869−873.

BI002050M